commentary

Critical assessment of charge mobility extraction in FETs

Hyun Ho Choi, Kilwon Cho, C. Daniel Frisbie, Henning Sirringhaus and Vitaly Podzorov

Mobility is an important charge-transport parameter in organic, inorganic and hybrid semiconductors. We outline some of the common pitfalls of mobility extraction from field-effect transistor (FET) measurements and propose practical recommendations to avoid reporting erroneous mobilities in publications.

Charge carrier mobility plays a central role in semiconductor science and technology, because the efficiency of semiconductor devices generally improves as charge mobilities increase. Correspondingly, materials research understandably focuses on strategies for improving mobility, which requires sound approaches for reproducible mobility measurements. Here we focus on field-effect transistor (FET)[1] measurements, because FETs are technologically relevant devices pervasive in the literature. There are a number of checks one must perform to ensure accurate extraction of the FET mobility. Failure to adhere to these guidelines has resulted in a number of reports of erroneous mobilities, particularly for organic field-effect transistors (OFETs). Our aim here is to articulate the best practices for mobility extraction from FET measurements, so that common pitfalls are avoided. It goes without saying that responsible reporting of mobility is of great importance to the materials research community, as any inflation of findings hinders further work, may misguide future research directions and threatens the credibility of the field. Although in this Commentary we use OFETs as examples, most of the considerations are not materials specific and apply also to other emergent semiconductors suitable for FET technologies, including inorganic oxides[2], hybrid perovskites[3], transition-metal dichalcogenides and other monolayer materials[4,5], as well as semiconductor nanocrystal arrays[6], nanowires and carbon nanotubes[7].

Mobility and common pitfalls

The practical importance of charge mobility, μ, in FETs stems from the fact that the higher the mobility, the greater the source–drain current, I_{SD}, realized in a FET within a certain span of the gate voltage, V_G, at a given source–drain voltage, V_{SD} (refs 8,9). However, this expectation is fulfilled only if FETs exhibit the expected linear relationship between the carrier density n and conductivity σ: $\sigma = \mu e n$, where e is electron charge. Stated another way, for μ to be a truly meaningful parameter, the linearity of FET transfer characteristics (that is, $I_{SD}(V_G)$ and $|I_{SD}|^{1/2}(V_G)$ dependences in the linear and saturation regimes, respectively) is very important. The equations for $I_{SD}(V_G, V_{SD})$ dependences in a FET (also called the Shockley equations) used for mobility extraction are derived within the gradual channel approximation based on the specific assumptions that (a) the transverse gate electric field is much greater than the longitudinal source–drain electric field, and (b) the mobility is carrier-density independent[1]. These assumptions lead to a FET model with linear transfer characteristics[8], in which the linear (μ_{lin}) and saturation (μ_{sat}) regime mobilities can be expressed as:

$$\mu_{lin,2p} = \frac{L}{WC_iV_{SD}}\left(\frac{\partial I_{SD}}{\partial V_G}\right) \text{ or}$$

$$\mu_{lin,4p} = \frac{D}{WC_i}\left(\frac{\partial(I_{SD}/V_{4p})}{\partial V_G}\right), \quad (1)$$

applicable at $|V_G - V_T| \gg |V_{SD}|$

$$\mu_{sat,2p} = \frac{2L}{WC_i}\left(\frac{\partial\sqrt{|I_{SD}|}}{\partial V_G}\right)^2, \quad (2)$$

applicable at $|V_G - V_T| < |V_{SD}|$

Here, the subscripts 2p and 4p refer to two-probe and four-probe measurements, L and W are the length and width of the accumulation channel, C_i is the gate-channel capacitance per unit area, V_{SD} and V_T are the source–drain and threshold voltages. V_{4p} is the voltage between the two voltage probes separated by the distance D along the channel in a gated four-probe configuration[8,10,11]. Equations (1) and (2) are only applicable when dependences $I_{SD}(V_G)$ in the linear regime and $|I_{SD}|^{1/2}(V_G)$ in the saturation regime are linear in an extended range of V_G. If FET transfer characteristics are nonlinear, μ obtained by using these equations only in a very limited linear range or at a point of high curvature is likely to be inaccurate — such a 'mobility' can serve as neither a useful device characteristic nor a material parameter.

In highly ordered systems such as single-crystal FETs, the device characteristics can closely resemble those of ideal FETs expected from the Shockley assumptions, and reliable μ values can be extracted from linear $I_{SD}(V_G)$ and $|I_{SD}|^{1/2}(V_G)$ graphs in the linear and saturation regimes, respectively, provided that other extrinsic sources of error, such as short-channel effects or high contact resistance, are excluded[9]. These mobilities may also be used to provide feedback to theoretical electronic structure calculations and validate charge-transport models[12–14].

In disordered systems, μ could be carrier-density dependent (for instance, due to band-tail filling)[15]; in such cases, equation (1) in the linear regime can still be used to extract the V_G-dependent mobility, provided that it is experimentally verified that the nonlinearities are not caused by contact effects or other device issues. In addition, μ extracted in practical thin-film devices typically reflects a combination of intrinsic and extrinsic factors that affect charge transport (including grain-boundary and charged-impurity scattering, gate dielectric inhomogeneity and carrier trapping), and theoretical models that aim at extracting the intrinsic materials properties should carefully take into account all these factors while making a comparison with experimental values. From a device perspective, the mobility estimated from

non-ideal transfer characteristics may still represent a useful tool to compare the ability of different device architectures to deliver high output currents and provide efficient modulation of conductance with gate voltage; yet several rules must be followed to ensure the reliability of these estimations.

In this Commentary, we outline the main sources of data misinterpretation in FETs, introduce a simple parameter — the measurement reliability factor r — that helps to quickly gauge the overall effectiveness of mobility claims in research articles, and propose a list of requirements that should be fulfilled to avoid basic artefacts in mobility measurements.

Figure 1 summarizes the common types of nonlinearities in FETs. The red dashed line corresponds to the highest slope that is sometimes erroneously used in mobility calculations. The black dashed line represents an electrically equivalent ideal FET (that is, a FET delivering the same maximum source–drain current $|I_{SD}|^{max}$ at the same maximum gate voltage $|V_G|^{max}$ as those in the reported experiment), but functioning as an ideal transistor well described by the Shockley FET equations (that is, a FET with a linear transfer characteristic and zero V_T). Please note that the mobility of such an electrically equivalent ideal FET (proportional to the slope of the black dashed line in Fig. 1) depends on the particular measurement parameters (for instance, $|V_G|^{max}$ and the shape of the transfer curve) and does not necessarily represents the intrinsic carrier mobility of the reported FET. Nonlinearities in Fig. 1a–c might have diverse microscopic origins (partially discussed in the recommendations below), including contact effects, carrier density-dependent mobility and non-equilibrium biasing of short-channel OFETs. A peculiar nonlinearity called a 'hump' (Fig. 1d), can lead to a peak in $\mu(V_G)$ curve near the threshold, followed by a plateau[16] (corresponding to the green dashed line in Fig. 1d). It was suggested that the hump originates from gated Schottky contacts, and the intrinsic carrier mobility corresponds to the plateau[16]. This was confirmed with more detailed measurements[17]. Similarly, double-slope characteristics in donor–acceptor polymer FETs, originating from minority carrier injection and trapping[18], can lead to features similar to the hump that are frequently misinterpreted as high carrier mobility in polymer FETs. More generally, the green dashed lines in Fig. 1d–f represent the suggested linear fits to the FET characteristics that can better estimate a meaningful value for the
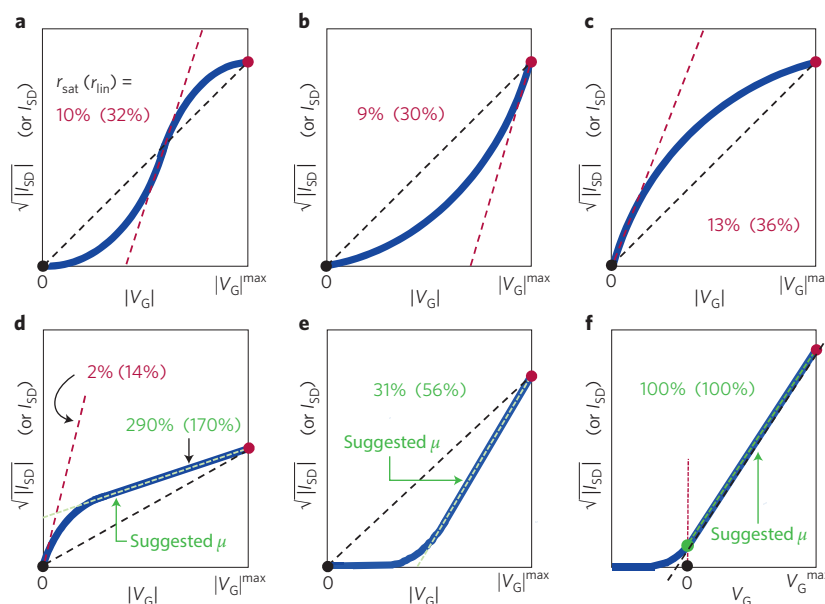

Figure 1 | Common nonlinearities in FET transfer characteristics. **a–f**, Transfer curves are schematically shown on linear-scale plots either for saturation or linear regime measurements. The plots assume $|V_{SD}| \ll |V_G|^{max}$ for the linear regime, or $|V_{SD}| > |V_G|^{max}$ for the saturation regime, where $|V_G|^{max}$ corresponds to the maximum gate voltage used in the measurements. S-shaped curve (**a**), superlinear curve (**b**), sublinear curve (**c**), a hump nonlinearity in the sub-threshold region with otherwise extended linear region (**d**), linear characteristic with a significant threshold (**e**), and close-to-ideal FET behaviour with a linear transfer characteristic and negligible threshold (**f**). The black dot represents the origin; the red dot at $|V_G|^{max}$ corresponds to the maximum channel conductivity experimentally reached in each case; the green dot (**f**) corresponds to the channel conductivity at $V_G = 0$ (I_{SD}^0 in Box 1). The red and green dashed lines indicate slopes used in calculations of the claimed mobility. The black dashed line represents the slope of an electrically equivalent ideal FET delivering the same maximum channel conductivity at $|V_G|^{max}$ but exhibiting correct linear characteristics, compliant with the standard Shockley FET equations[9]. The green dashed line in the extended linear region of the transfer characteristic (**d–f**) corresponds to μ most closely representing the intrinsic charge carrier mobility of the FETs (assuming that additional verifications via four-probe and/or Hall measurements were carried out as per the guidelines in the text). The measurement reliability factor (defined in detail in Box 1) in the linear regime, r_{lin}, is the ratio, expressed in %, of the slopes of the black and red dashed lines (**a–d**) or black and green dashed lines (**d–f**), and is shown in brackets in the panels. The values outside the brackets correspond to the reliability factor in the saturation regime, r_{sat}, equal to the same ratio squared (equations (B1) and (B2)). Parameter $r > 100\%$ (as in **d**) is a reflection of the fact that the device exhibits a hump-like nonlinearity.

device mobility. These lines fit extended linear regions of the transfer characteristic at a sufficiently high V_G, which can help avoiding some known sources of nonlinearity such as contact effects or minority carrier injection and trapping. Complementary gated four-probe or Hall effect measurements of mobility in devices with transfer characteristics as shown in Fig. 1d–f have confirmed a closer match with the μ values extracted from the green dashed lines[11,16,17,19,20]. Figure 1e represents FET behaviour fully consistent with the physical model of FET operation (the Shockley model): it features an extended linear region (fitted with a green dashed line), though with a substantial threshold. The mobility in this case can, in principle,

be reliably extracted from the slope of the green dashed line, and it will likely represent adequately the actual carrier mobility at the semiconductor/dielectric interface in a given FET. However, high V_T might be indicative of a high density of deep traps or problems with carrier injection, and therefore trap density and contact resistance must be thoroughly investigated, especially if a high μ is claimed. Finally, Fig. 1f represents a close-to-ideal FET with linear transfer characteristic and negligible V_T. In such a case, both the black and green dashed lines coincide with the data, making the extraction of μ unambiguous. Even in this case, two-probe mobility μ_{2p} might still be affected by contact resistance, and
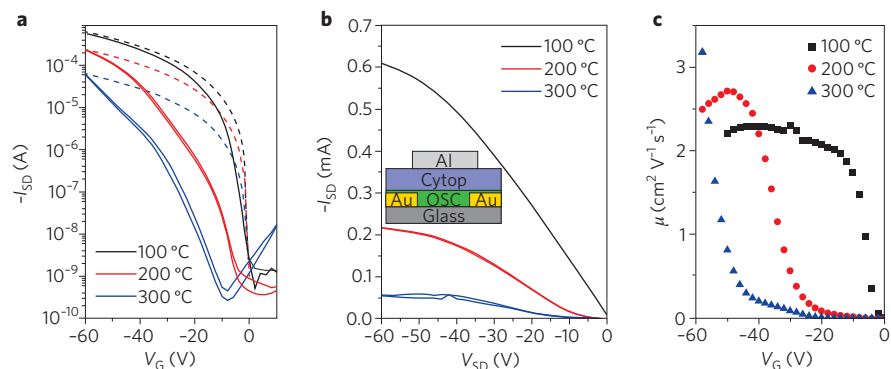
Figure 2 | Illustration of mobility extraction artefacts in devices with non-ideal characteristics. **a**, $I_{SD}(V_G)$ characteristics at $V_{SD} = -60$ V of conjugated polymer FETs based on indacenodithiophene-co-benzothiadiazole (IDTBT) films annealed at different temperatures (solid lines)[21]. The dashed lines show the ideal transistor characteristics corresponding to devices with effective mobility $\mu_{eff} = 2$ cm^2 V^{-1} s^{-1} (black), 0.75 cm^2 V^{-1} s^{-1} (red) and 0.2 cm^2 V^{-1} s^{-1} (blue), calculated according to the procedure described in Box 1 (equations (B1) and (B3)). The reliability factor is $r_{sat} = 86\%$ (100 °C), 26% (200 °C) and 6% (300 °C). **b**, Corresponding $I_{SD}(V_{SD})$ characteristics recorded at $V_G = -60$ V showing evidence for contact resistance limitations in the devices annealed at higher temperatures. The inset shows a cross-section of device structure consisting of an organic semiconductor with gold contacts, topped with a Cytop dielectric and an aluminium gate. **c**, V_G-dependent mobility extracted according to equation (2), showing unrealistic trends for μ values of devices annealed at 200 °C (red) and 300 °C (blue). Device parameters: $L = 20$ μm, $W = 1$ mm, the gate dielectric is a 500-nm-thick Cytop ($\varepsilon = 2.1$) with $C_i = 3.72$ nF cm^{-2}.

further four-probe FET measurements are desirable.

Figure 2 illustrates the kind of issues that can arise when applying equation (2) to non-ideal devices. It shows characteristics of polymer OFETs based on films annealed at different temperatures[21]. The films annealed at 100 °C exhibit nearly ideal saturation regime characteristics with a close to quadratic increase of I_{SD} with V_G and negligible V_T; in contrast, the devices annealed at 200 °C and 300 °C exhibit significant non-idealities with higher V_T and a stronger than quadratic increase of I_{SD} above the threshold. The 200 °C and 300 °C devices clearly exhibit inferior performance, as their I_{SD} is lower than that of the 100 °C device. The corresponding output characteristics in Fig. 2b show that the likely reason for this is an increased contact resistance. If equation (2) is applied to these characteristics, a reliable and nearly V_G-independent mobility of 2 cm^2 V^{-1} s^{-1} is extracted for the 100 °C device, whereas significantly overestimated values are obtained at high V_G for the 200 °C and 300 °C devices (Fig. 2c). It is in fact intuitive that devices with lower ON current should not exhibit higher mobility. The origin of this problem is that in the 200 °C and 300 °C devices the increased contact resistance strongly suppresses the current at low V_G but leads to a more rapid increase in I_{SD} at higher V_G, hence resulting in overestimation of mobility.

A measurement reliability factor

To parameterize the set of issues presented in Fig. 1 in a unified way, we introduce the measurement reliability factor, r, designed to reveal the overall ability of a reported FET to deliver on its promise. This parameter is defined as the ratio (expressed in %) of the maximum channel conductivity experimentally achieved in a FET to the maximum channel conductivity expected in an equivalent but ideal FET (well described by the Shockley model) with the claimed mobility and zero threshold voltage: $r \equiv \sigma_{achieved}^{max} / \sigma_{ideal}^{max}$. It can be calculated from device parameters and characteristics reported in research articles as shown in Box 1, or found graphically by simply calculating the ratio of the slope of the black dashed line to the slope of the line used in the articles to calculate the claimed μ (for instance, the red or green dashed lines in Fig. 1). In the linear regime, r_{lin} is given by this ratio of slopes, whereas in the saturation regime, r_{sat} is given by the ratio squared. The reliability factor r is a useful metric that allows readers to quickly gauge the actual impact of each mobility claim by quantifying how much the claimed mobility differs from that of an electrically equivalent FET following the ideal Shockley behaviour and delivering the same maximum conductivity as the FET in question at the maximum gate voltage in the investigated V_G range. A close-to-ideal FET operation, well described by the

Shockley model, corresponds to $r = 100\%$, which thus allows the most unambiguous carrier mobility extraction. Cases of $r > 100\%$ (such as that for the hump or double-slope nonlinearities schematically shown in Fig. 1d) simply indicate that the studied devices have this specific type of non-ideality, and the mobility extracted from the green dashed line is either underestimated or sufficiently closely represents the intrinsic mobility of this semiconductor in a given FET, provided that additional measurements, such as a gated four-probe or Hall effect, were carried out in this V_G region and confirmed the longitudinal FET μ measurements. We suggest that evaluating FETs in terms of the reliability factor and explicitly reporting the obtained r in the research articles should become common practice. A number of recent OFET reports turn out to have quite low reliability factors, while r can get well above 75% in high-quality OFETs[22].

It is clear that evaluating the reliability factor only makes sense if particularly crude errors in mobility extraction are avoided. These include using erroneous channel dimensions (for instance, underestimated W or overestimated L/W ratio), underestimated gate-channel capacitance (for instance, $C_i = 10$ nF cm^{-2} is frequently used for 300-nm-thick thermal SiO$_2$, instead of the correct value of 11.5 nF cm^{-2}), or working with unpatterned semiconductors that lead to fringe currents. Saturation regime measurements should not be truncated at $|V_G| << |V_{SD}|$, otherwise they only probe a near-threshold region prone to nonlinearities. Finally, applying source–drain electric fields exceeding the breakdown field of air ($E_{brkd} = 3 \times 10^4$ V cm^{-1}) in top-contact FETs should be avoided, as this can make measurements unreliable.

Avoiding pitfalls

To ensure that FET mobility is extracted correctly, we recommend the following guidelines.

Linearity of FET transfer characteristics is important. Whenever possible μ should be extracted from transfer characteristics that are linear over a substantial range of gate voltage. That is, $I_{SD}(V_G)$ in the linear regime and $|I_{SD}|^{1/2}(V_G)$ in the saturation regime must be both linear. Linearity of these characteristics is prescribed by the Shockley FET equations[8], leading to V_G-independent μ, as in high-quality single-crystal OFETs[9,23] (see, for example, characteristics of rubrene OFETs in Fig. 3). Given the current physical understanding of the effect of disorder on charge transport and carrier mobility in organic semiconductors, a claim of a high

Box 1 | Calculating the measurement reliability factor, r, in FETs.

The goal of the measurement reliability factor, r, is to assess whether the behaviour of reported FETs follows the physics of the simple linear increase of conductivity with carrier density under the assumption of a constant mobility and negligible threshold voltage. It is defined as the ratio of the maximum channel conductivity experimentally achieved in a FET at the maximum gate voltage to the maximum channel conductivity expected in a correctly functioning ideal FET with the claimed carrier mobility μ and identical other device parameters at the same maximum gate voltage. It can be calculated from the claimed μ, the stated device parameters and the FET characteristics shown in papers. In the saturation regime, it is easy to show that the reliability factor is:

$$r_{sat} = \left(\frac{\sqrt{|I_{SD}|^{max}} - \sqrt{|I_{SD}^0|}}{|V_G|^{max}} \right)^2 \Bigg/ \left(\frac{WC_i}{2L} \mu_{sat} \right)_{claimed}$$

$$= \left(\frac{\sqrt{|I_{SD}|^{max}} - \sqrt{|I_{SD}^0|}}{|V_G|^{max}} \right)^2 \Bigg/ \left(\frac{\partial \sqrt{|I_{SD}|}}{\partial V_G} \right)^2_{claimed} \quad (B1)$$

Here, μ_{sat} is the mobility claimed in a paper, L, W and C_i are the claimed device parameters, and $|I_{SD}|^{max}$ is the experimental maximum source–drain current reached at the maximum gate voltage $|V_G|^{max}$ (red dot in Fig. 1). I_{SD}^0 denotes the source–drain current at $V_G = 0$. In most FETs based on undoped semiconductors, I_{SD}^0 is negligible and can be assumed to be zero (black dots in Fig. 1a–e). In a few cases, however, I_{SD}^0 can be substantial and should be taken into account. These include, for instance, FETs based on chemically doped semiconductors, or FETs with an electrostatic shift of the onset voltage occurring due to charged gate dielectrics, dipolar monolayers at the semiconductor–dielectric interface, or simply due to a substantial positive (negative) V_{SD} applied during the linear-regime measurements of the transfer characteristics in p-type (n-type) FETs. For all these cases, I_{SD}^0 is schematically represented by the green dot in Fig. 1f. The derivative in the denominator on the right-hand side of equation (B1) is the

slope used to calculate the claimed μ_{sat} (corresponding to the red or green dashed lines in Fig. 1). The value in the brackets in the numerator is the slope of an electrically equivalent FET behaving according to the ideal Shockley equations, given by the black dashed line in Fig. 1. Equation (B1) shows that r_{sat} is simply equal to the squared ratio of the slope of an electrically equivalent FET to the slope actually used to calculate the claimed μ.

Similarly, in the linear regime, the reliability factor is:

$$r_{lin} = \left(\frac{||I_{SD}|^{max} - |I_{SD}^0||}{|V_G|^{max}} \right) \Bigg/ \left(\frac{|V_{SD}| WC_i}{L} \mu_{lin} \right)_{claimed}$$

$$= \left(\frac{||I_{SD}|^{max} - |I_{SD}^0||}{|V_G|^{max}} \right) \Bigg/ \left(\left| \frac{\partial I_{SD}}{\partial V_G} \right| \right)_{claimed} \quad (B2)$$

Again, r_{lin} can be either calculated from the claimed mobility μ_{lin} and declared experimental parameters or simply found graphically. In the case of the green dashed line in Fig. 1d, $r > 100\%$ simply reflects the fact that the device exhibits a hump nonlinearity. According to the meaning of reliability factor, having $r > 100\%$ makes sense in this case, since an ideal FET with μ defined by the slope of the green dashed line would deliver a lower maximum conductivity than the actual device of this type.

The measurement reliability factor can be used to define an effective carrier mobility of a reported FET that represents its equivalent electrical performance:

$$\mu_{eff} \equiv r \times \mu_{claimed} \quad (B3)$$

Indeed, a FET following the ideal Shockley equations with mobility μ_{eff} would deliver the same overall electrical performance as the reported nonlinear device with the claimed mobility $\mu_{claimed}$. This is illustrated in Fig. 2a with the dashed lines. Examples of reliability factor r, as well as the maximum current density j_{SD}^{max} and power P_{max} in FETs channel (equations (3) and (4)), calculated for selected literature reports can be found in ref. 22.

---

absolute mobility ($\mu > 1$ cm^2 V^{-1} s^{-1}) would be inconsistent with simultaneously having a strong dependence of μ on carrier density (and V_G)[9,14,15]. When linear characteristics cannot be obtained even after extensive device optimization, we propose that (a) μ should only be extracted from linear-regime measurements (equation (1)), (b) contact resistance must be characterized (see below), (c) the observation of a behaviour far from the ideal Shockley equations should be explicitly acknowledged, and (d) the reliability factor r should be quoted. We also recommend that (e) authors show the fit to experimental output characteristics ($I_{SD}(V_{SD})$ curves measured at several V_G values in the range $0 < |V_G| < |V_{SD}|^{max}$) using the Shockley FET model with the claimed μ: such fits are important as they easily show how well the devices are described by the gradual channel model.

Linear regime is strongly preferred for μ extraction in FETs. Linear-regime mobility,

μ_{lin}, should be listed in papers as the primary charge carrier mobility. A comparison with the saturation regime measurement, μ_{sat}, can be made. Measurements in saturation regime are more prone to erroneous mobility extraction, especially when μ is a function of n (refs 8,9), because n strongly varies along the channel, and there is a pinch-off region near one of the contacts that may result in a non-uniform distribution of the longitudinal electric field. In FETs with n-independent μ and negligible contact resistance, μ_{lin} and μ_{sat} should match[9] (Fig. 3c).

Contact resistance in FETs should be addressed. It was shown particularly in OFETs that Schottky contact resistance, R_C, can lead to nonlinear device characteristics[8,17]. The commonly used FET equations (equations (1) and (2) for μ_{2p}) assume that $R_C = 0$, and applying them to OFETs affected by contacts would lead to inaccurate μ. Efficient methods of addressing

contact resistance are the gated four-probe measurements introduced in organic electronics for the first time in single-crystal OFETs[10,11,24,25] and a transmission-line method[8]. Besides these measurements, yielding R_C and a contact-corrected μ, a simple test for severity of contact effects is a V_{SD}-scaling check: in the linear regime, FETs that are not significantly affected by contacts should exhibit I_{SD} proportional to V_{SD} (that is, V_{SD}-independent σ and μ_{2p})[11], as shown in Fig. 3a.

Hysteresis and V_G sweep-rate dependence of μ in FETs should be characterized. Devices with significant disorder, charge trapping or other instabilities may exhibit a nominal μ varying by more than an order of magnitude with the rate of V_G sweep, making an assignment of a single mobility value to these devices futile[26]. Thus, reports of high-performance FETs should include characterization of V_G sweep-rate dependence of μ performed at rates
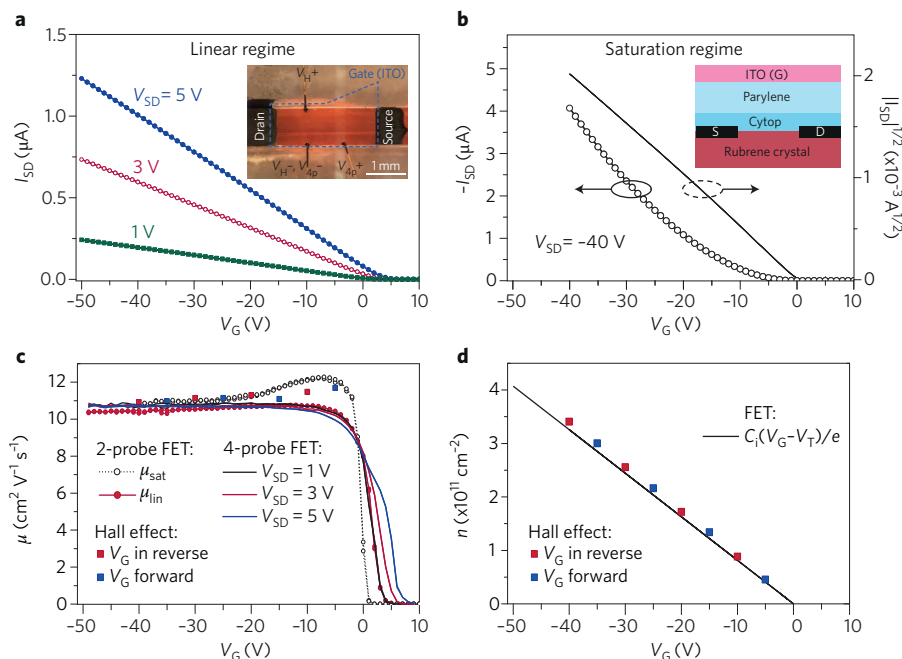
Figure 3 | FET and Hall effect measurements in single-crystal rubrene OFET. **a**, Linear-regime $I_{SD}(V_G)$ recorded at $V_{SD} = 1$, 3 and 5 V. The inset shows a photograph of the FET ($L = 2.5$ mm, $L/W = 2.76$). **b**, Saturation-regime $I_{SD}(V_G)$ (open symbols, left axis) and $|I_{SD}|^{1/2}(V_G)$ (solid line, right axis) recorded at $V_{SD} = -40$ V. The inset shows the device structure: rubrene crystal with graphite contacts is coated with a gate dielectric (50 nm of Cytop, $\varepsilon = 2.1$, topped with a 1.828-μm-thick parylene-N, $\varepsilon = 2.65$) and a 50-nm-thick ITO gate[9]. **c**, Two-probe mobility in the saturation (open black circles) and linear (solid red circles) regimes, four-probe mobility in the linear regime at $V_{SD} = 1$, 3 and 5 V (solid lines) (calculated according to equations (1) and (2))[9], and Hall mobility (solid squares)[19]. **d**, Measured Hall carrier density (symbols) compared to the capacitively defined carrier density (solid line)[19]. The capacitance measured in test structures $C_i = 1.24$ nF cm^{-2} agrees with the calculated C_i within 5%. The maximum current density in the OFET's channel is $j_{SD}^{max} = 44$ A cm^{-2} and 150 A cm^{-2} in the linear and saturation regimes, respectively. All measurements are performed in air, at 300 K, with V_G slowly swept back and forth in closed loops at a rate 0.5 V s^{-1} (~4 min per curve), revealing negligible hysteresis. A very good match between Hall and FET mobilities and carrier densities indicates that the Hall effect is fully developed, with charge carriers behaving like mobile (coherent) band carriers. The reliability factor $r_{sat} = r_{lin} = 100\%$.

spanning at least an order of magnitude, including the low rate of ~1 V s^{-1}, approaching the d.c. operation. In addition, hysteresis in $I_{SD}(V_G)$ and $|I_{SD}|^{1/2}(V_G)$ should be shown, and μ averaged over the entire hysteresis loop should be quoted.

All information necessary for mobility evaluation must be explicitly listed. Researchers should show FET transfer characteristics on double-linear plots and include the gate-channel capacitance C_i, the channel width, W, and length, L, V_G sweep rate and all other essential parameters. A photograph of the FET corresponding to the representative measurement should be included. In cases of multilayer gate dielectrics or single-component polymer dielectrics, C_i should be measured and compared with the expected value; any significant deviations should be addressed. This would allow the interested readers to

reproduce the mobility values reported in the articles.

Extra caution must be taken when measuring FETs with constricted channels. One should avoid using FETs based on individual nano/microwires or ribbons, or, more generally, FETs with very short or narrow channels, unless special care is taken to ensure that the devices are: (a) not contact-limited (that is, Schottky contact resistance is much lower than the channel resistance in the V_G range used for mobility extraction), and (b) maintained at thermal and electrical equilibrium during measurements. The pitfalls of measuring such devices are associated with high local electric fields, current densities and Joule heat emitted in a very small volume of the sample that can lead to poorly controlled, nonlinear or unstable device characteristics. For instance, applying very high V_{SD} (up to

100 V) across short (5–50 μm) or narrow (a few μm) channels, leading to enormous current densities and electric fields, is rather common in OFETs. One can estimate the maximum current density, j_{SD}^{max}, in a FET's channel as:

$$j_{SD}^{max} \equiv |I_{SD}|^{max}/(Wd_0) \qquad (3)$$

where $|I_{SD}|^{max}$ is the maximum absolute source–drain current shown in papers, W is the channel width and d_0 is the accumulation layer thickness of a few molecular layers (for definitiveness, we take $d_0 = 3$ nm). In several recent studies, very high current densities beyond 10^4–10^5 A cm^{-2} were driven through OFETs, which might have been the reason for nonlinear characteristics[22]. Such j_{SD}^{max} are more than an order of magnitude greater than the fire safety allowance of 1.2 kA cm^{-2} or even the fusing (melting) threshold of 10 kA cm^{-2} for domestic 18-AWG (diameter 1.024 mm) electrical copper wiring[27]. Analogously, one can estimate the maximum power density emitted in reported FETs as:

$$P_{max} \equiv |I_{SD}|^{max} \times |V_{SD}|/(WL) \qquad (4)$$

revealing that P_{max} significantly exceeds 100 W cm^{-2} in a number of recent reports[22]. For comparison, a typical household iron emits ~ 0.36 W cm^{-2} at a full-power operation. Although OFETs can withstand brief applications of high j and P, the timescale of such measurements is crucial, yet measurement rates are rarely reported. To avoid data misinterpretation due to these extreme biasing conditions, we propose that researchers performing OFET measurements at $j > 10^3$ A cm^{-2} (a) quote measurement timescale (V_G sweep rate)[26], (b) make sure that transfer characteristics are linear (that is, compliant with equations (1) and (2)), or otherwise reduce excitation voltage/current, and (c) quote the reliability factor r. In linear-regime measurements of short-channel ($L < 100$ μm) FETs, it is recommended to limit V_{SD} to a few volts. For instance, only a few volts were applied to the 2.5-mm-long channel of rubrene OFET in Fig. 3, resulting in equilibrium transport with very low $j_{SD}^{max} < 0.2$ kA cm^{-2} and $P_{max} \approx 7$ mW cm^{-2} (equations (3) and (4)), yet a high $\mu \approx 11$ cm^2 V^{-1} s^{-1}.

Hall-effect measurements are highly desirable when $\mu > 5$ cm^2 V^{-1} s^{-1} is claimed. Hall measurements are very useful in supporting the observation of high FET mobilities, particularly in organic semiconductors[28–30], as they provide evidence that charge transport occurs (at least partially) through delocalized states[19]. It is expected that at such level

of μ most homogeneous semiconductors would exhibit the so-called fully developed Hall effect with $n_{Hall} \approx n_{FET}$ and $\mu_{Hall} \approx \mu_{FET}$ (ref. 19), similarly to other high-mobility OFETs[28–30]. An example of this behaviour is shown in Fig. 3c,d. If a self-consistent dataset can be obtained by satisfying most of the other items of these guidelines, Hall measurements may not be necessary. On the contrary, if FETs still exhibit unconventional characteristics (nonlinearities, double-slopes, hysteresis and so on) even after efforts on device optimization, we encourage researchers to attempt Hall measurements to confirm the mobility estimated with FET measurements. More generally, Hall measurements would provide an important means to determine if carriers in the studied system behave as expected in conventional band semiconductors.

Outlook

We have assessed critically how the application of widely used methods for extracting FET mobilities to devices with non-ideal characteristics can lead to significant mobility overestimation. To improve the reliability of mobility extraction in organic and inorganic FETs we would like to make the following practical recommendations.

First, errors in the parameters that enter into the mobility extraction need to be minimized. This includes accurate measurements of channel geometry (L and W), the minimization of current spreading by semiconductor patterning and the use of correct gate dielectric capacitance measured at sufficiently low frequencies ($f < 100$ Hz). These parameters should be reported in each publication.

As a second recommendation, the reliability factor r (equations (B1) and (B2))

should be reported in publications and the effective mobility (equation (B3)) should be used as the practical figure of merit for assessing FET performance.

Finally, whenever possible, measurements should be conducted under conditions that optimize the reliability factor around 100% and maximize the effective mobility. Following the guidelines suggested above as closely as possible, the reliability of the mobility values reported in the scientific literature may be significantly improved.

FETs based on organic semiconductors, oxides, as well as nanostructured and monolayer materials have witnessed impressive progress over the last decade, bringing these devices closer to becoming a serious technology for a wide range of electronics applications. It is thus becoming increasingly important to assess mobilities realistically and reliably, such that other important frontier challenges, including achieving a sound understanding of structure–property relationships in new materials, improving operational device stability, as well as integration of FETs into flexible and stretchable electronics, could be addressed more efficiently. We hope that these recommendations will help to establish procedures for measuring progress in materials and device performance in these exciting cross-fertilized fields in a robust and reliable manner. ❏

Hyun Ho Choi and Vitaly Podzorov are in the Department of Physics, Rutgers University, 136 Frelinghuysen Road, Piscataway, New Jersey 08854, USA. Kilwon Cho and H.H.C. are in the Department of Chemical Engineering, Pohang University of Science and Technology (POSTECH), Pohang 37673, South Korea. C. Daniel Frisbie is in the Department of Chemical Engineering and Materials Science, University of Minnesota, 421 Washington Avenue SE, Minneapolis, Minnesota 55455, USA. Henning Sirringhaus is at the Cavendish Laboratory, University of Cambridge, JJ Thomson Avenue, Cambridge CB3 0HE, UK.

References

1. Sze, S. M. & Ng, K. K. *Physics of Semiconductor Devices* 3rd edn (Wiley, 2007).
2. Xie, W., Zhang, X., Leighton, C. & Frisbie, C. D. *Adv. Electron. Mater.* **3**, 1600369 (2017).
3. Chen, Y. *et al. Nat. Commun.* **7**, 12253 (2016).
4. Podzorov, V., Gershenson, M. E., Kloc, Ch., Zeis, R. & Bucher, E. *Appl. Phys. Lett.* **84**, 3301–3303 (2004).
5. Schmidt, H., Giustiniano, F. & Eda, G. *Chem. Soc. Rev.* **44**, 7715–7736 (2015).
6. Jang, J., Liu, W., Son, J. S. & Talapin, D. V. *Nano Lett.* **14**, 653–662 (2014).
7. Sun, D.-m. *et al. Nat. Nanotech.* **6**, 156–161 (2011).
8. Bao, Z. & Locklin, J. *Organic Field-Effect Transistors* Ch. 2 (CRC press, 2007).
9. Podzorov, V. *MRS Bull.* **38**, 15–24 (2013).
10. Podzorov, V., Pudalov, V. M. & Gershenson, M. E. *Appl. Phys. Lett.* **82**, 1739–1741 (2003).
11. Podzorov, V., Sysoev, S. E., Loginova, E., Pudalov, V. M. & Gershenson, M. E. *Appl. Phys. Lett.* **83**, 3504–3506 (2003).
12. Troisi, A. & Orlandi, G. *Phys. Rev. Lett.* **96**, 086601 (2006).
13. Sánchez-Carrera, R. S., Paramonov, P., Day, G. M., Coropceanu, V. & Brédas, J.-L. *J. Am. Chem. Soc.* **132**, 14437–14446 (2010).
14. Fratini, S., Mayou, D. & Ciuchi, S. *Adv. Funct. Mater.* **26**, 2292–2315 (2016).
15. Xia, Y., Cho, J. H., Lee, J., Ruden, P. P. & Frisbie, C. D. *Adv. Mater.* **21**, 2174–2179 (2009).
16. Yi, H. T., Chen, Y., Czelen, K. & Podzorov, V. *Adv. Mater.* **23**, 5807–5811 (2011).
17. Bittle, E. G., Basham, J. I., Jackson, T. N., Jurchescu, O. D. & Gundlach, D. J. *Nat. Commun.* **7**, 10908 (2016).
18. Okachi, T., Kashiki, T. & Ohya, K. *Proc. SPIE* **9568**, 95680I (2015).
19. Yi, H. T., Gartstein, Y. N. & Podzorov, V. *Sci. Rep.* **6**, 23650 (2016).
20. Uemura, T. *et al. Adv. Mater.* **28**, 151–155 (2016).
21. Nikolka, M. *et al. Nat. Mater.* **16**, 356–362 (2017).
22. Choi, H. H., Cho, K., Frisbie, C. D., Sirringhaus, H. & Podzorov, V. *Zenodo* https://doi.org/10.5281/zenodo.1050698 (2017).
23. Ren, X. *et al. Adv. Electron. Mater.* **3**, 1700018 (2017).
24. Takeya, J. *et al. J. Appl. Phys.* **94**, 5800–5804 (2003).
25. Newman, C. R., Chesterfield, R. J., Merlo, J. A. & Frisbie, C. D. *Appl. Phys. Lett.* **85**, 422–424 (2004).
26. Chen, Y. *et al. Phys. Chem. Chem. Phys.* **14**, 14142–14151 (2012).
27. https://en.wikipedia.org/wiki/American_wire_gauge
28. Podzorov, V., Menard, E., Rogers, J. A. & Gershenson, M. E. *Phys. Rev. Lett.* **95**, 226601 (2005).
29. Uemura, T. *et al. Curr. Appl. Phys.* **12**, S87–S91 (2012).
30. Xie, W., Wang, S., Zhang, X., Leighton, C. & Frisbie, C. D. *Phys. Rev. Lett.* **113**, 246602 (2014).

TABLE. The measurement reliability factor, *r*, in FET publications.

Critical assessment of charge mobility extraction in field-effect transistors.

(Aug. 1, 2017)

Hyun Ho Choi[1,2], Kilwon Cho[2], C. Daniel Frisbie[3], Henning Sirringhaus[4], and Vitaly Podzorov[1]

[1] Department of Physics, Rutgers University, 136 Frelinghuysen Rd., Piscataway, NJ 08854, USA.
[2] Department of Chemical Engineering, Pohang University of Science and Technology (POSTECH), Pohang 37673, South Korea.
[3] Department of Chemical Engineering and Materials Science, University of Minnesota, 421 Washington Ave SE, Minneapolis, MN 55455, USA.
[4] Cavendish Laboratory, University of Cambridge, J. J. Thomson Ave, Cambridge CB3 0HE, UK.

TABLE. The measurement reliability factor, *r*, the maximum power density, P_{max}, dissipated in the transistor channel and the maximum current density, j_{SD}^{max}, in the channel of OFETs in recent literature reports.

- *r* is defined as the ratio of experimentally reached maximum conductivity to the maximum conductivity expected in the correctly working FET (characterized with linear transconductance and zero threshold) that has the claimed carrier mobility. For the exact definition of *r* see *Nature Mater*. DOI: 10.1038/nmat5035. The goal of *r* is to gauge mobility claims in literature by assessing whether the behavior of reported devices is following the physics of the linear increase of conductivity with carrier density under the assumption of a constant mobility.

- P_{max} is defined as the maximum electric power dissipated in the channel of the reported FET per unit area, $P_{max} \equiv (|I_{SD}|^{max} \cdot |V_{SD}|)/(L \cdot W)$.

- j_{SD}^{max} is estimated as the maximum source-drain current, I_{SD}^{max}, ran through the FET divided by the product $W \cdot d_0$, where W is the channel width and d_0 is the accumulation layer thickness (taken for definitiveness to be $d_0 \equiv 3$ nm (a few molecular layers) for OFETs): $j_{SD}^{max} \equiv |I_{SD}|^{max}/(W \cdot d_0)$.

Reference	semicond./ins.	Fig.	$\mu_{claimed}$ $(cm^2V^{-1}s^{-1})$	*r* (%)	P_{max} $(W \cdot cm^{-2})$ *	j_{SD}^{max} $(kA \cdot cm^{-2})$ †	comments
Y. Yuan *et al.*, *Nat. Commun.* (2014)[1]	C$_8$-BTBT:PS / PVP:HDA	4a	25 (sat.)	13	14 (Fig. 4e)	11.7 (Fig. 4e)	Highly non-linear characteristics, high threshold voltage.
C. Liu *et al.*, *J. Phys. Chem. C* (2013)[2]	C$_8$-BTBT/SiO$_2$ C$_8$-BTBT/Cytop	2a 2d	1.7 (sat.) 2 (sat.)	90.4 73	3.8 1.6	9.6 4.0	Linear characteristics, low threshold voltage.
H. Li *et al.*, *J. Am. Chem. Soc.* (2012)[3]	C$_{60}$ / BCB-covered SiO$_2$	4b 4e	10.3 (sat.) 4.5 (sat.)	22 9	341 164	56.8 21.4	Highly non-linear characteristics.
J.-m. Cho *et al.*, *Appl. Phys. Lett.* (2015)[4]	C$_8$-BTBT / PMMA	1c	16.1 (sat)	16	10.4	12.2	Highly non-linear characteristics, very high threshold voltage.

*** For comparison, the working surface of a typical household clothes iron emits about 0.36 W·cm^{-2} at a full-power operation.**

† For comparison, the fire safety allowance for domestic 18-AWG copper wire (diameter 1.024 mm) at normal conditions is about 1.2 kA·cm^{-2}, and its fusing (melting) threshold is about 10 kA·cm^{-2}.

TABLE. The measurement reliability factor, r, in FET publications.

Reference	semicond./ins.	Fig.	$\mu_{claimed}$ (cm^{2}V^{-1}s^{-1})	r (%)	P_{max} (W·cm^{-2})*	j_{SD}^{max} (kA·cm^{-2})†	comments
G. Giri et al., Nature (2011)[5]	TIPS-pentacene / PTS-treated SiO$_2$	4c	4.6 (sat)	13	125	21	Highly non-linear characteristics, significant thresholds. Underestimated C_i was used in μ calculations.
D. He et al., Nat. Commun. (2014)[6]	C$_8$-BTBT/h-BN	4a S32a	10 (lin.) 5 (lin.)	38 31	0.3 0.14	2.4 1.0	High threshold voltage; Large disparity between lin. and sat. μ: $\mu_{sat} = 0.34$ cm^{2}V^{-1}s^{-1} (Fig. 4b) and $\mu_{sat} = 0.065$ cm^{2}V^{-1}s^{-1} (Fig. S33b).
H. T. Yi et al., Adv. Mater. (2011)[7]	rubrene / insulating polymers	2A	4.7 (lin.) for $\varepsilon = 2.26$ 4.4 (sat.) for $\varepsilon = 2.26$	~ 100	3.3×10^{-3}	0.07	Linear transfer characteristics, negligible threshold voltage ($L = 1$ mm, $W = 1.5$ mm).
E. Menard et al., Adv. Mater. (2004)[8]	rubrene/air	3c 3a	10.7 (lin.) 13.5 (lin.)	~ 100 ~ 85	9.3×10^{-2} 1.5×10^{-2}	0.5 0.15	Linear characteristics with zero or low threshold voltage.
B. Blülle et al., Phys. Rev. Appl. (2014)[9]	rubrene/Cytop	2 3	13 (lin.) 13.9 (sat.)	~ 100 ~ 100	7×10^{-2} 0.3	0.6 1.0	Linear characteristics, negligible thresholds.
W. Xie et al., J. Phys. Chem. C (2013)[10]	D-rubrene/air	3c	13.9 (lin.)	86	5.6×10^{-3}	0.1	Linear characteristics, very low thresholds.
N. A. Minder et al., Adv. Mater. (2012)[11]	PDIF-CN$_2$/air	1c	2.8 (lin.)	70	2.4×10^{-3}	0.02	Linear characteristics, some threshold.
J. Li et al., Sci. Rep. (2012)[12]	DPP-DTT-based D-A polymer / alkylated-SiO$_2$	2d,g	8 (sat.)	34	14	7.6	Highly non-linear characteristics.
Q. Wang et al., Adv. Funct. Mater. (2016)[13]	C$_8$-BTBT / bare SiO$_2$	S7a	13 (sat.)	13	7.9	12	Non-linear characteristics, very high thresholds. Large disparity between lin. and sat. regimes: $\mu_{sat} = 4.8$ cm^{2}V^{-1}s^{-1} in Fig. 8b, but $\mu_{lin} = 2.34$ cm^{2}V^{-1}s^{-1} in Fig. 8c.
J.-m. Cho, T. Mori, Phys. Rev. Appl. (2016)[14]	Ph-BTBT-C$_{10}$/ SiO$_2$	2a	13 (sat.)	10	2.3	10	Non-linear characteristics, very high thresholds.
H. Iino et al., Nat. Commun. (2015)[15]	Ph-BTBT-C$_{10}$/ SiO$_2$	3b	14.7 (sat.)	23	180	60	Linear characteristics, high threshold voltage with much extended subthreshold region. Underestimated C_i was used in μ calculations.
H. Chen et al., Adv. Mater. (2012)[16]	PDVT-10 D-A polymer / alkylated-SiO$_2$	1c	8.0 (sat.)	< 13	52	8.6	$|I_{SD}|^{1/2}$ vs. V_G characteristics are truncated at $|V_G| \ll |V_{SD}|$, thus limiting data to near-threshold region. The upper bound of r is estimated by linear extrapolation of the shown portion of the transfer curve to $|V_G| = |V_{SD}|$.
H.-R. Tseng et al., Adv. Mater. (2014)[17]	PCDTPT polymer / alkylated-SiO$_2$	1c	23.7 (sat.)	< 30	160	53	Same as above (truncated data).
C. Luo et al., Nano Lett. (2014)[18]	PCDTPT polymer / alkylated-SiO$_2$	4c	25.4 (sat.)	< 50	123	41	Same as above (truncated data).
J. Lee et al., J. Am. Chem. Soc. (2013)[19]	PTDPPSe-Si D-A polymer / alkylated-SiO$_2$	5d	5.97 (sat.)	30	423	71	μ is extracted from highly non-linear subthreshold region.

TABLE. The measurement reliability factor, r, in FET publications.

Reference	semicond./ins.	Fig.	$\mu_{claimed}$ (cm^{2}V^{-1}s^{-1})	r (%)	P_{max} (W·cm^{-2}) *	j_{SD}^{max} (kA·cm^{-2}) †	comments
J. Liu *et al.*, *Nat. Commun.* (2015)[20]	DPA / alkylated-SiO$_2$	3a	30 (sat.)	17	992	91	Non-linear transfer curves; very high threshold voltage. Ratio $L/W = 5$ used in μ calculation is inconsistent with the "micrometre or submicrometre organic ribbon" masking technique. Source-drain electric fields exceeding the breakdown field of air ($E_{SD} > 3\times10^4$ V·cm^{-1}) are used in these top-contact OFETs.
S. Kwon *et al.*, *Adv. Mater.* (2015)[21]	C$_8$-BTBT:PSS / alkylated-SiO$_2$	4b	4 (sat.)	65	55.5	31	Unpatterned channel allowing fringe currents is used. Noticeable threshold and hysteresis. $W = 1$ mm used for the interdigitated contact structure is underestimated by a factor of 2. $\mu_{claimed}$, P_{max} and j_{SD}^{max} are calculated from the data shown for the best device, but using the correct $W = 2$ mm.
X. Ren *et al.*, *Adv. Electron. Mater.* (2017)[22]	^{13}C-rubrene/air	2b	15.3 (lin.)	83	3.2×10^{-3}	0.06	Highly linear characteristics, low threshold voltage.
A. S. Molinari *et al.*, *J. Am. Chem. Soc.* (2009)[23]	PDIF-CN$_2$ / vacuum	2B	1 - 6 (lin.)	~ 100	0.9	15	Linear characteristics, negligible threshold.
J. Takeya *et al.*, *J. Appl. Phys.* (2003)[24]	pentacene / alkylated-SiO$_2$	2	0.1 - 0.5 (lin.)	90-100	8 (Fig. 2a)	0.7 (Fig. 2a)	Linear characteristics, negligible threshold.
H. Klauk *et al.*, *J. Appl. Phys.* (2002)[25]	pentacene / alkylated-SiO$_2$	5	1 (sat.)	~ 100	0.7	1.6	Linear characteristics, negligible threshold.
T. Uemura *et al.*, *Adv. Mater.* (2016)[26]	C$_{10}$-DNTT / alkylated-SiO$_2$	2b 2Sg	5.8 - 5.9 (lin.)	~ 100	17 (Fig. 2Sh)	22 (Fig. 2Sh)	Linear characteristics, negligible threshold. $\mu_{claimed}$ is calculated from the data shown, but using the correct $C_i = 34.5$ nF·cm^{-2} for 100 nm-thick SiO$_2$.
C. Rolin *et al.*, *Nat. Commun.* (2017)[27]	C$_8$-BTBT/SAM-treated SiO$_2$ C$_{10}$-DNTT / SAM-treated SiO$_2$ C$_{10}$-DNBDT / SAM-treated SiO$_2$	5 5 5	3.9 (lin.) 6.5 (lin.) 7.2 (lin.)	68 83 83	390 (Fig. S2)	91 (Fig. S2)	Linear characteristics, some thresholds.
Y. Krupskaya *et al.*, *Adv. Mater.* (2015)[28]	F$_2$-TCNQ / vacuum	1b	6 - 7 (lin.)	85-90	1.0	0.75	Linear characteristics, some thresholds. P_{max} and j_{SD}^{max} are calculated assuming $L \sim W \sim 0.16$ mm.
Y. Diao *et al.*, *Nat. Mater.* (2013)[29]	TIPS-pentacene / alkylated-SiO$_2$	5b	8.1 (sat.) 2.3 (sat.)	19 24	341 81	57 13	Highly non-linear characteristics.

3

TABLE. The measurement reliability factor, r, in FET publications.

Reference	semicond./ins.	Fig.	μ_{claimed} $(\text{cm}^2\text{V}^{-1}\text{s}^{-1})$	r (%)	P_{max} (W·cm^{-2}) *	$j_{\text{SD}}^{\text{max}}$ (kA·cm^{-2}) †	comments
I. Kang *et al.*, *Adv. Mater.* (2013)[30]	PDPPTSE / alkylated-SiO_2	3	4.97 (sat.)	2	0.5	0.9	Mobility is extracted from highly non-linear subthreshold region; significant *off*-state conductivity.
A. Zhang *et al.*, *Macromolecules* (2016)[31]	PDPP4T-2M / alkylated-SiO_2	3c	9.95 (sat. at low V_G) 1.0 (sat. at high V_G)	22 216	386	64	Non-linear transfer curves. Plots are truncated at $|V_G| < |V_{SD}|$.
J. Huang *et al.*, *Chem. Mater.* (2016)[32]	PAIID-BT-C3 / alkylated-SiO_2	4b	6.43 (sat.)	8	50	8.4	Highly sublinear characteristics.
F. Yang *et al.*, *Org. Electron.* (2016)[33]	PMDPP2T-DTT / alkylated-SiO_2	2b	5.32 (sat. at low V_G) 1.01 (sat. at high V_G)	26 147	378	50	Non-linear transfer curves.
Y.-Q. Zheng *et al.*, *Adv. Mater.* (2016)[34]	F_4BDOPV-2T / alkylated-SiO_2	3b	14.9 (sat.)	2	12	4.2	Mobility is extracted from highly non-linear subthreshold region; significant *off*-state conductivity.
M. Seifrid *et al.*, *Adv. Mater.* (2017)[35]	PCPDTBT derivative / alkylated-SiO_2	2b	8.5×10^{-3} (sat.)	100	4.1×10^{-2}	0.04	Linear characteristics, low threshold.
T. Lei *et al.*, *Adv. Mater.* (2012)[36]	IIDDT-C3 / alkylated-SiO_2	3a	1.92 (sat.)	20	62	12	Mobility is extracted from highly non-linear subthreshold region.
Y. Li *et al.*, *J. Am. Chem. Soc.* (2011)[37]	PDQT / alkylated-SiO_2	4d	1.0 (sat.)	43	13	6.3	Sub-linear characteristics.
H.-R. Tseng *et al.*, *Nano Lett.* (2012)[38]	PCDTBT / alkylated-SiO_2	3c	6.7 (sat.)	65	1255	209	Non-linear transfer characteristics with substantial *off*-state current.

REFERENCES:

1 Yuan, Y., Giri, G., Ayzner, A. L., Zoombelt, A. P., Mannsfeld, S. C., Chen, J., Nordlund, D., Toney, M. F., Huang, J., Bao, Z. Ultra-high mobility transparent organic thin film transistors grown by an off-centre spin-coating method. *Nat. Commun.* **5**, 3005 (2014). https://www.nature.com/articles/ncomms4005

2 Liu, C., Xu, Y., Li, Y., Scheideler, W., Minari, T. Critical impact of gate dielectric interfaces on the contact resistance of high-performance organic field-effect transistors. *J. Phys. Chem. C* **117**, 12337-12345 (2013). http://pubs.acs.org/doi/abs/10.1021/jp4023844

3 Li, H., Tee, B. C.-K., Cha, J. J., Cui, Y., Chung, J. W., Lee, S. Y., Bao, Z. High-mobility field-effect transistors from large-area solution-grown aligned C_{60} single crystals. *J. Am. Chem. Soc.* **134**, 2760-2765 (2012). http://pubs.acs.org/doi/abs/10.1021/ja210430b

4 Cho, J.-m., Higashino, T., Mori, T. Band-like transport down to 20 K in organic single-crystal transistors based on dioctylbenzothienobenzothiophene. *Appl. Phys. Lett.* **106**, 193303 (2015). http://aip.scitation.org/doi/abs/10.1063/1.4921343

TABLE. The measurement reliability factor, *r*, in FET publications.

[5] Giri, G., Verploegen, E., Mannsfeld, S. C. B., Atahan-Evrenk, S., Kim, D. H., Lee, S. Y., Becerril, H. A., Aspuru-Guzik, A., Toney, M. F., Bao, Z. Tuning charge transport in solution-sheared organic semiconductors using lattice strain. *Nature* **480**, 504-508 (2011). https://www.nature.com/nature/journal/v480/n7378/abs/nature10683.html

[6] He, D., Zhang, Y., Wu, Q., Xu, R., Nan, H., Liu, J., Yao, J., Wang, Z., Yuan, S., Li, Y., Shi, Y., Wang, J., Ni, Z., He, L., Miao, F., Song, F., Xu, H., Watanabe, K., Taniguchi, T., Xu, J. B., Xinran, W. Two-dimensional quasi-freestanding molecular crystals for high-performance organic field-effect transistors. *Nat. Commun.* **5**, 5162 (2014). https://www.nature.com/articles/ncomms6162

[7] Yi, H. T., Chen, Y., Czelen, K., Podzorov, V. Vacuum Lamination Approach to Fabrication of High-Performance Single-Crystal Organic Field-Effect Transistors. *Adv. Mater.* **23**, 5807-5811 (2011). http://onlinelibrary.wiley.com/doi/10.1002/adma.201103305/full

[8] Menard, E., Podzorov, V., Hur, S. H., Gaur, A., Gershenson, M. E., Rogers, J. A. High-Performance n-and p-Type Single-Crystal Organic Transistors with Free-Space Gate Dielectrics. *Adv. Mater.* **16**, 2097-2101 (2004). http://onlinelibrary.wiley.com/doi/10.1002/adma.200401017/abstract

[9] Blülle, B., Häusermann, R., Batlogg, B. Approaching the trap-free limit in organic single-crystal field-effect transistors. *Phys. Rev. Appl.* **1**, 034006 (2014). https://journals.aps.org/prapplied/abstract/10.1103/PhysRevApplied.1.034006

[10] Xie, W., McGarry, K. A., Liu, F., Wu, Y., Ruden, P. P., Douglas, C. J., Frisbie, C. D. High-Mobility Transistors Based on Single Crystals of Isotopically Substituted Rubrene-d_{28}. *J. Phys. Chem. C* **117**, 11522-11529 (2013). http://pubs.acs.org/doi/abs/10.1021/jp402250v

[11] Minder, N. A., Ono, S., Chen, Z., Facchetti, A., Morpurgo, A. F. Band-Like Electron Transport in Organic Transistors and Implication of the Molecular Structure for Performance Optimization. *Adv. Mater.* **24**, 503-508 (2012). http://onlinelibrary.wiley.com/doi/10.1002/adma.201103960/full

[12] Li, J., Zhao, Y., Tan, H. S., Guo, Y., Di, C.-A., Yu, G., Liu, Y., Lin, M., Lim, S. H., Zhou, Y., Su, H., Ong, B. S. A stable solution-processed polymer semiconductor with record high-mobility for printed transistors. *Sci. Rep.* **2**, 754 (2012). https://www.nature.com/articles/srep00754

[13] Wang, Q., Qian, J., Li, Y., Zhang, Y., He, D., Jiang, S., Wang, Y., Wang, X., Pan, L., Wang, J., Wang, X., Hu, Z., Nan, H., Ni, Z., Zheng, Y., Shi, Y. 2D Single-Crystalline Molecular Semiconductors with Precise Layer Definition Achieved by Floating-Coffee-Ring-Driven Assembly. *Adv. Funct. Mater.* **26**, 3191-3198 (2016). http://onlinelibrary.wiley.com/doi/10.1002/adfm.201600304/full

[14] Cho, J.-m., Mori, T. Low-Temperature Band Transport and Impact of Contact Resistance in Organic Field-Effect Transistors Based on Single-Crystal Films of Ph-BTBT-C$_{10}$. *Phys. Rev. Appl.* **5**, 064017 (2016). https://journals.aps.org/prapplied/abstract/10.1103/PhysRevApplied.5.064017

[15] Iino, H., Usui, T., Hanna, J.-i. Liquid crystals for organic thin-film transistors. *Nat. Commun.* **6**, 6828 (2015). https://www.nature.com/articles/ncomms7828

[16] Chen, H., Guo, Y., Yu, G., Zhao, Y., Zhang, J., Gao, D., Liu, H., Liu, Y. Highly π-Extended Copolymers with Diketopyrrolopyrrole Moieties for High-Performance Field-Effect Transistors. *Adv. Mater.* **24**, 4618-4622 (2012). http://onlinelibrary.wiley.com/doi/10.1002/adma.201201318/full

TABLE. The measurement reliability factor, *r*, in FET publications.

[17] Tseng, H. R., Phan, H., Luo, C., Wang, M., Perez, L. A., Patel, S. N., Ying, L., Kramer, E. J., Nguyen, T. Q., Bazan, G. C., Heeger, A. J. High-Mobility Field-Effect Transistors Fabricated with Macroscopic Aligned Semiconducting Polymers. *Adv. Mater.* **26**, 2993-2998 (2014). http://onlinelibrary.wiley.com/doi/10.1002/adma.201305084/full

[18] Luo, C., Kyaw, A. K. K., Perez, L. A., Patel, S., Wang, M., Grimm, B., Bazan, G. C., Kramer, E. J., Heeger, A. J. General strategy for self-assembly of highly oriented nanocrystalline semiconducting polymers with high mobility. *Nano Lett.* **14**, 2764-2771 (2014). http://pubs.acs.org/doi/abs/10.1021/nl500758w

[19] Lee, J., Han, A.-R., Yu, H., Shin, T. J., Yang, C., Oh, J. H. Boosting the ambipolar performance of solution-processable polymer semiconductors via hybrid side-chain engineering. *J. Am. Chem. Soc.* **135**, 9540-9547 (2013). http://pubs.acs.org/doi/abs/10.1021/ja403949g

[20] Liu, J., Zhang, H., Dong, H., Meng, L., Jiang, L., Jiang, L., Wang, Y., Yu, J., Sun, Y., Hu, W., Heeger, A. J. High mobility emissive organic semiconductor. *Nat. Commun.* **6**, 10032 (2015). https://www.nature.com/articles/ncomms10032

[21] Kwon, S., Kim, J., Kim, G., Yu, K., Jo, Y. R., Kim, B. J., Kim, J., Kang, H., Park, B., Lee, K. Organic Single-Crystal Semiconductor Films on a Millimeter Domain Scale. *Adv. Mater.* **27**, 6870-6877 (2015). http://onlinelibrary.wiley.com/doi/10.1002/adma.201502980/full

[22] Ren, X., Bruzek, M. J., Hanifi, D. A., Schulzetenberg, A., Wu, Y., Kim, C. H., Zhang, Z., Johns, J. E., Salleo, A., Fratini, S., Troisi, A., Douglas, C. J., Frisbie, C. D. Negative Isotope Effect on Field-Effect Hole Transport in Fully Substituted ^{13}C-Rubrene. *Adv. Electron. Mater.* **3**, 1700018 (2017). http://onlinelibrary.wiley.com/doi/10.1002/aelm.201700018/full

[23] Molinari, A. S., Alves, H., Chen, Z., Facchetti, A., Morpurgo, A. F. High Electron Mobility in Vacuum and Ambient for PDIF-CN$_2$ Single-Crystal Transistors. *J. Am. Chem. Soc.* **131**, 2462-2463 (2009). http://pubs.acs.org/doi/abs/10.1021/ja809848y

[24] Takeya, J., Goldmann, C., Haas, S., Pernstich, K. P., Ketterer, B., Batlogg, B. Field-induced charge transport at the surface of pentacene single crystals: A method to study charge dynamics of two-dimensional electron systems in organic crystals. *J. Appl. Phys.* **94**, 5800-5804 (2003). http://aip.scitation.org/doi/abs/10.1063/1.1618919

[25] Klauk, H., Halik, M., Zschieschang, U., Schmid, G., Radlik, W., Weber, W. High-mobility polymer gate dielectric pentacene thin film transistors. *J. Appl. Phys.* **92**, 5259-5263 (2002). http://aip.scitation.org/doi/abs/10.1063/1.1511826

[26] Uemura, T., Rolin, C., Ke, T.-H., Fesenko, P., Genoe, J., Heremans, P., Takeya, J. On the Extraction of Charge Carrier Mobility in High-Mobility Organic Transistors. *Adv. Mater.* **28**, 151-155 (2016). http://onlinelibrary.wiley.com/doi/10.1002/adma.201503133/abstract

[27] Rolin, C., Kang, E., Lee, J.-H., Borghs, G., Heremans, P., Genoe, J. Charge carrier mobility in thin films of organic semiconductors by the gated van der Pauw method. *Nat. Commun.* **8**, 14975 (2017). https://www.nature.com/articles/ncomms14975

[28] Krupskaya, Y., Gibertini, M., Marzari, N., Morpurgo, A. F. Band-like electron transport with record-high mobility in the TCNQ family. *Adv. Mater.* **27**, 2453-2458 (2015). http://onlinelibrary.wiley.com/doi/10.1002/adma.201405699/full

TABLE. The measurement reliability factor, *r*, in FET publications.

[29] Diao, Y., Tee, B. C. K., Giri, G., Xu, J., Kim, D. H., Becerril, H. A., Stoltenberg, R. M., Lee, T. H., Xue, G., Mannsfeld, S. C. B., Bao, Z. Solution coating of large-area organic semiconductor thin films with aligned single-crystalline domains. *Nat. Mater.* **12**, 665-671 (2013). http://www.nature.com/nmat/journal/v12/n7/abs/nmat3650.html

[30] Kang, I., An, T. K., Hong, J.-a., Yun, H.-J., Kim, R., Chung, D. S., Park, C. E., Kim, Y.-H., Kwon, S.-K. Effect of Selenophene in a DPP Copolymer Incorporating a Vinyl Group for High-Performance Organic Field-Effect Transistors. *Adv. Mater.* **25**, 524-528 (2013). http://onlinelibrary.wiley.com/doi/10.1002/adma.201202867/abstract

[31] Zhang, A., Xiao, C., Wu, Y., Li, C., Ji, Y., Li, L., Hu, W., Wang, Z., Ma, W., Li, W. Effect of Fluorination on Molecular Orientation of Conjugated Polymers in High Performance Field-Effect Transistors. *Macromolecules* **49**, 6431-6438 (2016). http://pubs.acs.org/doi/abs/10.1021/acs.macromol.6b01446

[32] Huang, J., Mao, Z., Chen, Z., Gao, D., Wei, C., Zhang, W., Yu, G. Diazaisoindigo-Based Polymers with High-Performance Charge-Transport Properties: From Computational Screening to Experimental Characterization. *Chem. Mater.* **28**, 2209-2218 (2016). http://pubs.acs.org/doi/abs/10.1021/acs.chemmater.6b00154

[33] Yang, F., Li, C., Zhang, J., Feng, G., Wei, Z., Li, W. Methylated conjugated polymers based on diketopyrrolopyrrole and dithienothiophene for high performance field-effect transistors. *Org. Electron.* **37**, 366-370 (2016). http://www.sciencedirect.com/science/article/pii/S156611991630310X

[34] Zheng, Y.-Q., Lei, T., Dou, J.-H., Xia, X., Wang, J.-Y., Liu, C.-J., Pei, J. Strong Electron-Deficient Polymers Lead to High Electron Mobility in Air and Their Morphology-Dependent Transport Behaviors. *Adv. Mater.* **28**, 7213-7219 (2016). http://onlinelibrary.wiley.com/doi/10.1002/adma.201600541/abstract

[35] Seifrid, M., Ford, M. J., Li, M., Koh, K. M., Trefonas, P., Bazan, G. C. Electrical Performance of a Molecular Organic Semiconductor under Thermal Stress. *Adv. Mater.* **29**, 1605511 (2017). http://onlinelibrary.wiley.com/doi/10.1002/adma.201605511/abstract

[36] Lei, T., Dou, J.-H., Pei, J. Influence of Alkyl Chain Branching Positions on the Hole Mobilities of Polymer Thin-Film Transistors. *Adv. Mater.* **24**, 6457-6461 (2012). http://onlinelibrary.wiley.com/doi/10.1002/adma.201202689/abstract

[37] Li, Y., Sonar, P., Singh, S. P., Soh, M. S., van Meurs, M., Tan, J. Annealing-Free High-Mobility Diketopyrrolopyrrole–Quaterthiophene Copolymer for Solution-Processed Organic Thin Film Transistors. *J. Am. Chem. Soc.* **133**, 2198-2204 (2011). http://pubs.acs.org/doi/abs/10.1021/ja1085996

[38] Tseng, H.-R., Ying, L., Hsu, B. B. Y., Perez, L. A., Takacs, C. J., Bazan, G. C., Heeger, A. J. High mobility field effect transistors based on macroscopically oriented regioregular copolymers. *Nano Lett.* **12**, 6353-6357 (2012). http://pubs.acs.org/doi/abs/10.1021/nl303612z